Editors' Suggestion

# Exact Numerical Solution of the Fully Connected Classical and Quantum Heisenberg Spin Glass

Nikita Kavokine,[1,2,*] Markus Müller,[3] Antoine Georges,[4,1,5,6] and Olivier Parcollet[1,7]
[1]Center for Computational Quantum Physics, Flatiron Institute, 162 5th Avenue, New York, New York 10010, USA
[2]Department of Molecular Spectroscopy, Max Planck Institute for Polymer Research, Ackermannweg 10, 55128 Mainz, Germany
[3]Paul Scherrer Institut, CH-5232 Villigen PSI, Switzerland
[4]Collège de France, Université PSL, 11 place Marcelin Berthelot, 75005 Paris, France
[5]Centre de Physique Théorique, Ecole Polytechnique, CNRS, Institut Polytechnique de Paris, 91128 Palaiseau Cedex, France
[6]DQMP, Université de Genève, 24 quai Ernest Ansermet, CH-1211 Genève, Suisse
[7]Université Paris-Saclay, CNRS, CEA, Institut de Physique Théorique, 91191, Gif-sur-Yvette, France

(Received 12 January 2024; revised 9 May 2024; accepted 18 May 2024; published 2 July 2024)

We present the mean field solution of the quantum and classical Heisenberg spin glasses, using the combination of a high precision numerical solution of the Parisi full replica symmetry breaking equations and a continuous time quantum Monte Carlo algorithm. We characterize the spin glass order and its low-energy excitations down to zero temperature. The Heisenberg spin glass has a rougher energy landscape than its Ising analog, and exhibits a very slow temperature evolution of its dynamical properties. We extend our analysis to the doped, metallic Heisenberg spin glass, which displays unexpectedly slow spin dynamics, reflecting the proximity to the melting quantum critical point and its associated Sachdev-Ye-Kitaev Planckian dynamics.

DOI: 10.1103/PhysRevLett.133.016501

While the physics of classical and quantum Ising spin glasses has been rather thoroughly understood, glasses of Heisenberg (vector) spins have remained a difficult and largely unsolved problem, including especially its quantum version, which governs the local moments in randomly doped, strongly correlated materials.

The approach of Sachdev and Ye [1] (SY), which takes a double limit of a fully connected exchange model with SU(2) spins promoted to SU($M \gg 1$), has attracted a lot of attention, as it exhibits very interesting features in the $M = \infty$ limit. In a fermionic representation of the SU($M \to \infty$) generators, the spins do not freeze, but remain in a spin liquid state [1] similar to the related Sachdev-Ye-Kitaev model of randomly coupled Majorana fermions [2]. When expanding around $M = \infty$, it was conjectured that a transition into a glassy phase occurs at an exponentially small critical temperature $\log(T_g) \propto -\sqrt{M}$ [3], and a recent study has established that this phase displays full replica symmetry breaking (RSB) [4]. A glass phase with similar features was found to occur in the transverse field Ising model [5,6] and the related multicomponent quantum rotor models [7–9]. In contrast, for bosonic SU($M$) representations, a spin glass phase occurs even for $M = \infty$, albeit with one-step RSB [3,10].

There is a fundamental difference between glasses displaying full RSB and one-step RSB. The energy landscape of the former features marginally stable local minima with a gapless spectrum of excitations, while the latter display a fully stable, gapped ground state, lying far below the manifold of marginally stable excited states that trap the dynamics. Marginal stability is key to the dynamics and the physics of avalanches in full RSB systems [11]. Which of these two scenarios applies to the physically relevant Heisenberg SU(2), $S = 1/2$ spin glass is an open question. Exact diagonalization of small fully connected systems is limited by finite size effects [12,13]. Surprisingly, not much is known about the *classical* (large $S$) limit of the Heisenberg mean-field spin glass either, apart from the replica-symmetric analysis of Refs. [14,15].

The equilibrium quantum spin dynamics of the SY spin-liquid [1] is similar to that of a marginal Fermi liquid [16]. It was realized early on [17] that this opens a new perspective on "strange" metals, culminating in recent models in which disorder and strong interactions conspire to prevent the emergence of quasiparticles and lead to $T$-linear resistivity down to the lowest temperatures [2,18]. It has recently been shown that such a behavior is found in the quantum critical region around the melting point of a metallic SU(2) Heisenberg spin glass [19,20]. However,

it is not known how the quantum dynamics change within the metallic spin glass phase itself.

In this Letter, we answer these open questions and present a solution of the fully connected spin-1/2 Heisenberg spin glass throughout its ordered phase. In the quantum case, the model reduces to an impurity problem for the spin dynamics coupled to Parisi's equations for the spin glass order. The Heisenberg glass has a full RSB solution, whose structure, however, differs crucially from an Ising glass. The insulating quantum glass displays the universal spin dynamics found in all solvable mean-field quantum glasses with full RSB in the limit $T \to 0$, but deviations from it persist to surprisingly low temperatures. Upon doping, we find a metallic spin glass with unexpectedly slow spin dynamics, close to the SY dynamics that dominate the quantum critical melting point of the spin glass.

*Model and method.*—We consider $N$ spins $\mathbf{S}_i$ with all-to-all interactions, described by the Hamiltonian

$$\mathcal{H} = -\sum_{i<j} J_{ij} \mathbf{S}_i \cdot \mathbf{S}_j. \tag{1}$$

The $\mathbf{S}_i$ are either classical Heisenberg spins—vectors constrained to the three-dimensional sphere of radius $S = 1/2$—or quantum SU(2) spins $S$ [with $\mathbf{S}^2 = S(S+1)$]. We use $\hbar = k_B = 1$ and denote by $\ell = 3$ the number of spin components. $J_{ij}$ are Gaussian random couplings with zero mean and variance $J^2/N$. We obtain the equilibrium solution of this model using the replica method and Parisi's full RSB ansatz [21–26], as detailed in the Supplemental Material [27].

In brief, the mean field model is reduced to an effective single spin problem in a random frozen field $\mathbf{h}$ with distribution $\mathbb{P}(\mathbf{h})$. In the classical case, it is governed by the Hamiltonian $H_{\rm loc}(\mathbf{h}) = -\mathbf{h} \cdot \mathbf{S}$. In the quantum case, the dynamics of this spin also depend on the self-averaging spin autocorrelation function $\chi(\tau) = \langle \mathbf{S}(0)\mathbf{S}(\tau)\rangle - \langle \mathbf{S}\rangle^2$, via the action

$$\mathcal{S}_{\rm loc}(\mathbf{h}) = \frac{J^2}{2} \int \int_0^\beta \mathrm{d}\tau \mathrm{d}\tau' \chi(\tau - \tau') \mathbf{S}(\tau) \cdot \mathbf{S}(\tau') - \mathbf{h} \int_0^\beta \mathrm{d}\tau\, \mathbf{S}(\tau), \tag{2}$$

where $\tau$ is Matsubara imaginary time and $\beta = 1/T$ the inverse temperature. The glass phase is described by an order parameter $q(x)$ ($x \in [0,1]$). $q(x)$ characterizes the distribution of phase space distances between local minima of the free energy landscape [25]. It determines the local field distribution $\mathbb{P}(\mathbf{h}) \equiv \mathbb{P}(x = 1, \mathbf{h})$, which is found by solving Parisi's equations for the magnetization $\mathbf{s}(x, \mathbf{h})$ and frozen fields distribution $\mathbb{P}(x, \mathbf{h})$

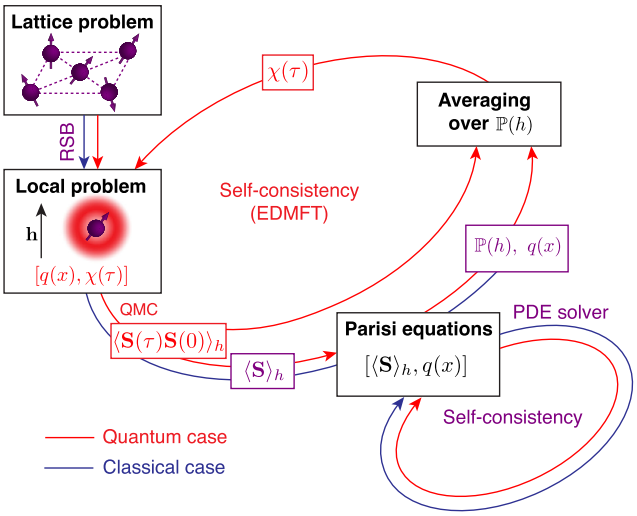


FIG. 1. Illustration of the algorithm to solve (2)–(5). In the classical case, the local problem is solved only once, and $q(x)$ is obtained solving Parisi's partial differential equations. In the quantum case, it is solved iteratively with CTQMC.

$$\frac{\partial \mathbf{s}}{\partial x} = -\frac{J^2}{2}\frac{\mathrm{d}q}{\mathrm{d}x}\left(\boldsymbol{\nabla}^2 \mathbf{s} + 2\beta x (\mathbf{s}\cdot\boldsymbol{\nabla})\mathbf{s}\right), \tag{3a}$$

$$\frac{\partial \mathbb{P}}{\partial x} = \frac{J^2}{2}\frac{\mathrm{d}q}{\mathrm{d}x}\left(\boldsymbol{\nabla}^2 \mathbb{P} - 2\beta x \boldsymbol{\nabla}(\mathbf{s}\cdot\mathbb{P})\right), \tag{3b}$$

$$\mathbf{s}(1, \mathbf{h}) = \langle \mathbf{S}\rangle_{H_{\rm loc}(\mathbf{h})|\mathcal{S}_{\rm loc}(\mathbf{h})}, \tag{3c}$$

$$\mathbb{P}(0, \mathbf{h}) = \delta(\mathbf{h}). \tag{3d}$$

These equations are solved self-consistently, with

$$q(x) = \frac{1}{\ell}\int \mathrm{d}\mathbf{h}\, \mathbb{P}(x, \mathbf{h}) \mathbf{s}(x, \mathbf{h})^2, \tag{4}$$

and, in the quantum case,

$$\chi(\tau) = \frac{1}{\ell}\int \mathrm{d}\mathbf{h}\, \mathbb{P}(\mathbf{h}) \langle \mathbf{S}(0)\mathbf{S}(\tau)\rangle_{\mathcal{S}_{\rm loc}(\mathbf{h})} - q(1). \tag{5}$$

Such self-consistency conditions are an example of extended dynamical mean-field theory (EDMFT) [5,28–30]. The iterative procedure to solve them is summarized in Fig. 1. A similar procedure has recently been implemented for mean field versions of transverse field Ising and quantum Coulomb glasses [6,31]. In contrast to the classical case, the single site quantum problem (2) cannot be solved analytically. Its solution is obtained with a "CTSEG" continuous-time quantum Monte Carlo (CTQMC) algorithm [27,32], without fermionic sign problem. The Parisi equations are solved with a high precision numerical method [error bars on

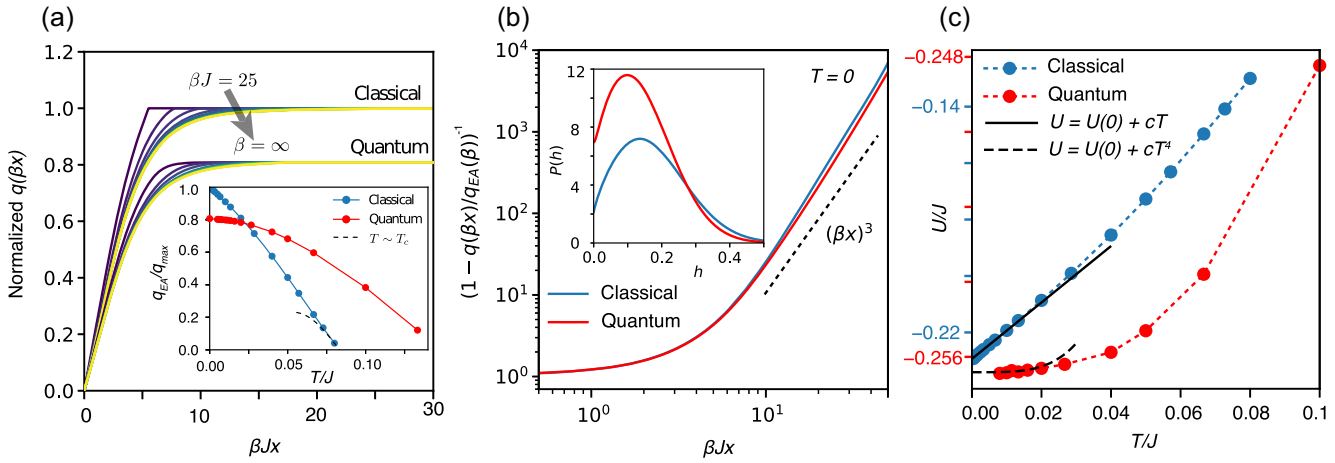


FIG. 2. Characteristics of the glass phase. (a) Overlap function $q(x)/q_{\rm EA}(\beta)$, normalized by $q_{\rm EA}(T=0)/q_{\rm max}$, for a range of temperature values, from $\beta J = 25$ to $\beta = \infty$. At low enough temperature, $q(x)/q_{\rm EA}(\beta)$ depends only on $\beta x$. Inset: $q_{\rm EA}$ vs $T$. The dashed line is the result of [34], valid for $T \approx T_{\rm g}$. (b) $1 - q(x)/q_{\rm EA}(T=0)$ at $T=0$, showing the power law approach to $q_{\rm EA}$ at large $\beta x$. Inset: local field distribution $\mathbb{P}(h)$ at zero temperature. (c) Internal energy as a function of temperature, with a fit for the classical case $U(T) - U(0) = cT$ ($c = 1 \pm 0.1$), and for the quantum case $U(T) - U(0) = cT^4$.

$q(x)$ being of order $10^{-5}$], using their integral form [33] and filtering methods to suppress numerical instabilities at low $T$ [27].

*Glass phase.*—A spin glass phase appears below a critical temperature $T_{\rm g}$, where the Edwards-Anderson order parameter $q_{\rm EA} \equiv q(x=1)$ turns on, as illustrated on Fig. 2(a). Our results for $T_{\rm g}$ are consistent with previous analytical work: $T_{\rm g} = JS^2/3$ ($\approx 0.08J$ for $S^2 = 1/4$) in the classical case [34] and $T_{\rm g} \approx J\langle \mathbf{S}^2 \rangle / 3\sqrt{3} \approx 0.15J$ in the quantum case [22], with $q_{\rm EA}(T)$ following the prediction of [34] close to $T_{\rm g}$ [Fig. 2(a), inset]. Note that $T_{\rm g}$ is higher in the quantum case, since the quantum spins are larger [$S(S+1) > S^2$].

For $T \ll T_{\rm g}$, the overlap function $q(x)$ obeys an approximate scaling form $q(x,T) = q_{\rm EA}(T) f(x/T) + O(T/J)$ [Figs. 2(a) and S13]. The function $f$ is determined by solving the Parisi equations (3a) and (3b) directly at $T=0$, upon changing to the natural variable $u = \beta x$. In the quantum case, they require as a boundary condition the zero temperature magnetizatio, $\langle \mathbf{S}(\tau) \rangle_{\mathcal{S}_{\rm loc}(\mathbf{h})}$, which we approximate by our lowest temperature QMC results (see [27] Figs. S5–S6). The results for $q(x)$ are shown in Figs. 2(a) and 2(b). The maximal possible overlap is $q_{\rm max} = \langle \mathbf{S}^2 \rangle / \ell$, corresponding to a product state without fluctuations. As expected, the classical glass approaches this value at $T=0$, while quantum fluctuations weakly reduce the order parameter to $q_{\rm EA} \approx 0.81 q_{\rm max}$ (consistent with exact diagonalization in Ref. [12], while the fit of spin correlations in Ref. [13] likely underestimated the order).

Unlike in the Ising case, local stability does not require a pseudogap in the distribution of local fields. Instead $\mathbb{P}(\mathbf{h}=0)$ remains finite and $\mathbb{P}(h) \approx \mathbb{P}(0) + ah$ [cf. Fig. 2(b)], since the probability of dangerously small fields is already suppressed by the phase space factor $\sim h^{\ell-1}$ [14,35]. This in turn is related to the tail of the overlap function $q(x)$. Indeed, (4) suggests that for $x$ close to 1, $q_{\rm EA} - q(x)$ counts the number of spins that see frozen fields of order $T/x$, for which one may expect $q_{\rm EA} - q(x) \sim \int_0^{T/x} {\rm d}h\, h^2 \mathbb{P}(h) \sim (T/x)^3 + O(T/x)^4$, consistent with an apparent power law: $\sim (T/x)^\alpha$. Numerically, we indeed find an apparent power-law approach: $1 - q(x)/q_{\rm EA} \sim 1/(\beta x)^\alpha$ as $T \to 0$, with $\alpha$ slightly larger than 3. This contrasts with the Ising case [5,25,35], where the linear pseudogap in $\mathbb{P}(h)$ leads to $\alpha = 2$. The lower density of small fields in the Heisenberg case suggests that low-lying metastable states have higher energies. This is consistent with the smaller value of the so-called break point $x_c$, above which $q(x)$ reaches a plateau ([27], Fig. S12). $T/x_c(T)$ can be interpreted as the typical free energy difference between the lowest metastable states [36]. While in the Ising case that energy scales linearly with $T$ as $x_c(T \to 0) \approx 0.5$ [35], in the Heisenberg glasses it decreases much more slowly as $T/x_c(T) \sim 1/\log(1/T)$, corroborating the picture of a rougher energy landscape. These differences will further show in the response to an increasing external field, under which the ground state magnetization increases in random discontinuous steps called "shocks." Their size distribution $\rho(\Delta m)$ was numerically found to be very similar to that of field-triggered out-of-equilibrium avalanches in the classical SK model [37,38], a phenomenon attributed to the marginal stability of the full RSB landscape. The equilibrium $\rho(\Delta m)$ is governed by the asymptotic approach of $q(x)$ to $q_{\rm EA}$. If it scales as $(T/x)^\alpha$, then $\rho(\Delta m) \sim 1/(\Delta m)^{2/\alpha}$ for $N^{-1/2} \ll \Delta m \ll 1$ [38]. For the classical Ising glass with $\alpha = 2$, $\rho(\Delta m) \propto 1/(\Delta m)$ exhibits a broad spectrum of avalanches. The larger $\alpha \approx 3$ of the

Heisenberg glasses leads to $\rho(\Delta m) \propto 1/(\Delta m)^{2/3}$, with predominant large scale rearrangements—as numerically observed in avalanches of XY ($\ell = 2$) spins [39].

*Specific heat.*—Let us now consider the internal energy per spin. In the classical case, it is given by [27]

$$U_{\mathrm{Cl}} = -\frac{\beta J^2 S^4}{2\ell}\left(1 - \frac{\ell^2}{S^4}\int_0^1 \mathrm{d}x\, q(x)^2\right). \tag{6}$$

In the quantum case, denoting $Q(\tau) = \chi(\tau) + q_{\mathrm{EA}}$ and $\bar{\tau} = \tau/\beta$, it reads

$$U_{\mathrm{Q}} = -\frac{\ell\beta J^2}{2}\left(\int_0^1 \mathrm{d}\bar{\tau}\, Q(\bar{\tau})^2 - \int_0^1 \mathrm{d}x\, q(x)^2\right). \tag{7}$$

As shown in Fig. 2(c), the classical and quantum internal energies behave very differently as a function of temperature. For classical vector spins, one expects a constant intrastate heat capacity $c = (\ell - 1)/2$ as $T \to 0$, each degree of freedom contributing $1/2$ by the equipartition theorem. A linear fit to our data yields $c \approx 1.0 \pm 0.1$, excluding sizable interstate contributions, consistently with finite-size simulations [40]. Quantum effects gap out the soft degrees of freedom and yield a much weaker temperature dependence of the internal energy [Fig. 2(c)]. A heat capacity proportional to $T^3$ was predicted for the SU($N$) quantum spin glass in the large $N$ limit, provided that marginally stable rather than equilibrium states are analyzed [41]. Our data are compatible with $U(T) \propto T^4$, but only at the lowest temperatures $T/J \lesssim 0.02$, as finite temperature corrections are substantial.

*Spin susceptibility.*—The spin-spin correlator $\chi(\tau)$ is shown in Fig. 3(a). For large $\tau$ it is well described by the conformal scaling form $\chi(\tau) \approx \chi(\beta/2)/[\sin(\pi\tau/\beta)]^{\theta}$ [17], implying that for $\omega \gtrsim T$, the dissipative part of the susceptibility at real frequencies $\chi''(\omega)$ scales as $\omega^{\theta-1}$. The exponent $\theta$ has significant, slow $T$ dependence [Fig. 3(b)]. Using a Landau expansion, Ref. [8] predicted that $\theta(T = 0) = 2$, [$\chi''(\omega) \propto \omega$]. This value was also found in a $1/M$ expansion of the SU($M$) quantum spin glass [4] and actually holds for all solvable cases of marginally stable states found so far [42]. From the limited numerically accessible temperature range, it is hard to unambiguously conclude whether $\lim_{T\to 0}\theta(T) = 2$. However, Fig. 3(b) suggests that this limit is indeed approached, albeit very slowly, as we can fit our data by $\theta(T) \approx 2\text{–}5.2 \times \sqrt{T/J}$. Interestingly, a similar behavior was found recently in the transverse-field Ising spin glass [6].

As discussed in Refs. [5,42], the low-$T$ behavior $c \propto T^3$, $\chi''(\omega) \propto \omega$ ($\theta = 2$) can be rationalized by approximating the eigenmodes of the Hessian describing the local curvature of the energy landscape as independent oscillators with spring constants $\lambda$ distributed as the eigenvalues of a random matrix $\rho(\lambda) \sim \sqrt{\lambda}$. For undamped oscillators of mass $M$, one has $M\omega^2 \sim \lambda$ with zero-point amplitudes given by $\lambda\langle x^2\rangle_\omega \sim \hbar\omega$, leading to $\chi''(\omega) \sim \rho(\omega)\langle x^2\rangle_\omega \sim \sqrt{M}\omega$. In this picture, an effective exponent $\theta < 2$ at finite $T$ may result from a $T$-dependent friction among modes. Assuming $\lim_{T\to 0}\theta(T) = 2$, we have $A \equiv \lim_{\omega\to 0}\chi''(\omega)/\omega \approx \lim_{\beta\to\infty}\beta^2\chi(\beta/2)/\pi$. We find $A \approx 3.5J^2$ and thus a significantly larger density of soft excitations than in the transverse field Ising spin glass, where $A \sim 0.5J^2$ (independent of the transverse field) was reported [5,6].

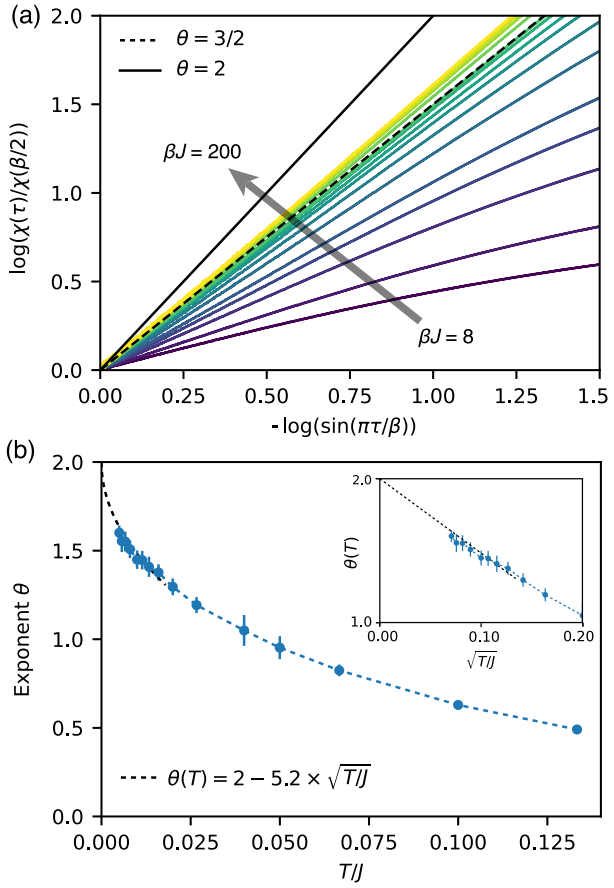


FIG. 3. Spin susceptibility. (a) Rescaled spin autocorrelation function in imaginary time, $\chi(\tau)/\chi(\beta/2)$, for a range of temperatures (from $\beta J = 8$ to $\beta J = 200$). At low temperature, it is well described by the conformal scaling form $\chi(\tau)/\chi(\beta/2) \approx [1/\sin(\pi\tau/\beta)]^{\theta}$, as shown by the linear behavior in the logarithmic plot. (b) Exponent $\theta$, obtained by fitting $Q(\tau)$ with the conformal scaling form, as a function of temperature. Inset: $\theta$ as a function of $\sqrt{T/J}$. The data are well described by $\theta(T) = 2\text{–}5.2 \times \sqrt{T/J}$ (black dashed line).

*Metallic quantum spin glass.*—In order to study the interplay between electrons and frozen spins arising from doping the spin glass, we use the Hamiltonian

$$\mathcal{H} = -\sum_{ij,\sigma=\uparrow,\downarrow} t_{ij} c^{\dagger}_{i\sigma} c_{j\sigma} + U\sum_i n_{i\uparrow} n_{i\downarrow} - \sum_{i<j} J_{ij}\mathbf{S}_i \cdot \mathbf{S}_j, \tag{8}$$

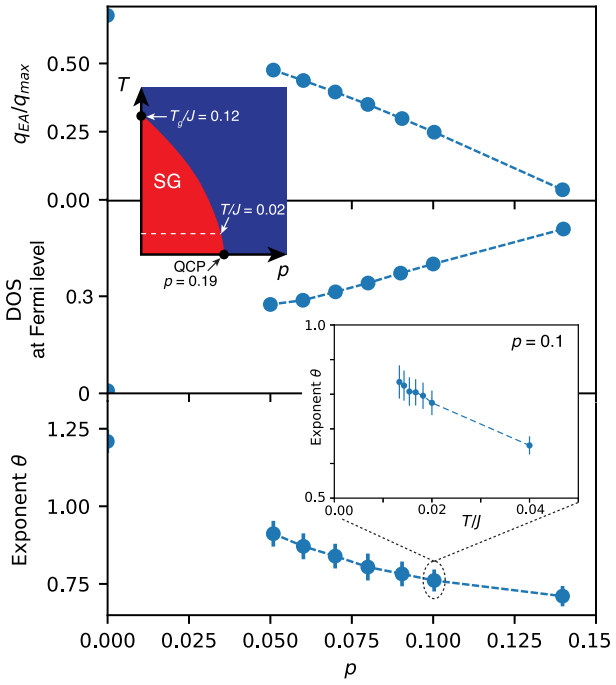


FIG. 4. Doped case. Glass order parameter $q_{\mathrm{EA}}$, density of states at the Fermi level, and scaling exponent $\theta$ of the spin-spin correlation function, as a function of doping $p$ at $\beta J = 50$. Dashed lines are guides to the eye. Upper inset: sketch of phase diagram. The spin glass (SG) melts at the quantum critical point (QCP). Lower inset: $\theta$ at fixed doping $p = 0.1$, as a function of temperature.

where $c_{i\sigma}$ and $c^{\dagger}_{i\sigma}$ are the electronic annihilation and creation operators, $n_{i\sigma} = c^{\dagger}_{i\sigma}c_{i\sigma}$, $\mathbf{S}^a_i = c^{\dagger}_{i\sigma}\boldsymbol{\sigma}^a_{\sigma\sigma'}c_{i\sigma'}$, and $U$ is the on-site electron-electron interaction. The hopping amplitudes $t_{ij}$ are randomly distributed with variance $t^2/N$. We denote the doping by $p = \langle n_\uparrow + n_\downarrow \rangle - 1$. This model has previously been solved in the paramagnetic phase [20]. Here, we solve the spin glass phase; as in [20], we use $U = 4t$ and $J = 0.5t$.

Below a critical doping $p_c$, a metallic spin glass appears, i.e., a phase with both a nonzero spin glass order parameter $q_{\mathrm{EA}}$ and a nonzero density of states at zero frequency, as illustrated in Fig. 4. This is compatible with the spin glass instability of the paramagnetic solution found in [20]. Previous studies of metallic quantum spin glasses have found a local spin susceptibility $\chi''(\omega) \propto \sqrt{\omega}$ corresponding to an exponent $\theta = 3/2$ at $T = 0$ [28,42,43]. This can be interpreted as originating from Ohmic damping of the oscillators in the physical picture discussed above. Intriguingly, we find that $\theta$ is smaller than unity for the whole range of (low) temperatures investigated. Our data do not appear consistent with $\theta$ reaching $3/2$ at $T = 0$ (possibly due to non-Ohmic damping by the non-Fermi-liquid metal) but may be consistent with $\theta$ reaching 1. The latter corresponds to the quantum critical dynamics found at the critical point $p = p_c$, which might extend through a large part of the metallic spin-glass phase.

In conclusion, we have solved the Heisenberg quantum spin glass for SU(2) spins. We found that the energy landscape of vector spins differs significantly from the Ising counterpart, resulting in different long time dynamics. Upon decreasing $T$, the short time quantum dynamics slowly approach the super-universal behavior of marginal mean field glasses, although featuring significantly softer collective modes and a lower freezing temperature than comparable Ising glasses. The marginal Fermi liquid-type quantum dynamics anticipated from the SU($M \gg 1$) approach is essentially absent in the undoped insulating limit of SU(2) spins, but appears to be present in a wide window influenced by the doping-induced quantum critical point in a metallic regime, that may be relevant for strongly correlated doped materials.

The data and code associated with the Letter are publicly available [44,45].

We thank Philipp Dumitrescu, Subir Sachdev, and Nils Wentzell for fruitful discussions. The Flatiron Institute is a division of the Simons Foundation. N. K. acknowledges support from a Humboldt fellowship. M. M. acknowledges support from SNSF Grant No. 200558.

*Contact author: nkavokine@flatironinstitute.org

[1] S. Sachdev and J. Ye, Phys. Rev. Lett. **70**, 3339 (1993).
[2] D. Chowdhury, A. Georges, O. Parcollet, and S. Sachdev, Rev. Mod. Phys. **94**, 035004 (2022).
[3] A. Georges, O. Parcollet, and S. Sachdev, Phys. Rev. B **63**, 134406 (2001).
[4] M. Christos, F. M. Haehl, and S. Sachdev, Phys. Rev. **105B**, 085120 (2022).
[5] A. Andreanov and M. Müller, Phys. Rev. Lett. **109**, 177201 (2012).
[6] A. Kiss, G. Zaránd, and I. Lovas, arXiv:2306.07337.
[7] J. Ye, S. Sachdev, and N. Read, Phys. Rev. Lett. **70**, 4011 (1993).
[8] N. Read, S. Sachdev, and J. Ye, Phys. Rev. B **52**, 384 (1995).
[9] M. Tikhanovskaya, S. Sachdev, and R. Samajdar, PRX Quantum **5**, 020313 (2024).
[10] A. Georges, O. Parcollet, and S. Sachdev, Phys. Rev. Lett. **85**, 840 (2000).
[11] M. Müller and M. Wyart, Annu. Rev. Condens. Matter Phys. **6**, 177 (2015).
[12] L. Arrachea and M. J. Rozenberg, Phys. Rev. Lett. **86**, 5172 (2001).
[13] H. Shackleton, A. Wietek, A. Georges, and S. Sachdev, Phys. Rev. Lett. **126**, 136602 (2021).
[14] A. J. Bray and M. A. Moore, J. Phys. C **14**, 2629 (1981).
[15] S. Franz, F. Nicoletti, G. Parisi, and F. Ricci-Tersenghi, SciPost Phys. **12**, 016 (2022).
[16] C. M. Varma, P. B. Littlewood, S. Schmitt-Rink, E. Abrahams, and A. E. Ruckenstein, Phys. Rev. Lett. **63**, 1996 (1989).

[17] O. Parcollet and A. Georges, Phys. Rev. B **59**, 5341 (1999).
[18] A. A. Patel, H. Guo, I. Esterlis, and S. Sachdev, Science **381**, 790 (2023).
[19] P. Cha, N. Wentzell, O. Parcollet, A. Georges, and E. A. Kim, Proc. Natl. Acad. Sci. U.S.A. **117**, 18341 (2020).
[20] P. T. Dumitrescu, N. Wentzell, A. Georges, and O. Parcollet, Phys. Rev. B **105**, L180404 (2022).
[21] D. Sherrington and S. Kirkpatrick, Phys. Rev. Lett. **35**, 1792 (1975).
[22] A. J. Bray and M. A. Moore, J. Phys. C **13**, L655 (1980).
[23] G. Parisi, J. Phys. A **13**, L115 (1980).
[24] B. Duplantier, J. Phys. A **14**, 283 (1981).
[25] M. Mézard, G. Parisi, and M. A. Virasoro, *Spin Glass Theory and Beyond* (World Scientific, Singapore, 1987), Chap. 3.
[26] A. Crisanti and T. Rizzo, Phys. Rev. E **65**, 046137 (2002).
[27] See Supplemental Material at http://link.aps.org/supplemental/10.1103/PhysRevLett.133.016501 for details of analytical calculations and supplementary figures.
[28] A. M. Sengupta and A. Georges, Phys. Rev. B **52**, 10295 (1995).
[29] J. L. Smith and Q. Si, Phys. Rev. B **61**, 5184 (2000).
[30] R. Chitra and G. Kotliar, Phys. Rev. Lett. **84**, 3678 (2000).
[31] I. Lovas, A. Kiss, C. P. Moca, and G. Zaránd, Phys. Rev. Res. **4**, 023067 (2022).
[32] J. Otsuki, Phys. Rev. B **87**, 125102 (2013).
[33] K. Nemoto, J. Phys. C **20**, 1325 (1987).
[34] M. Gabay, T. Garel, and C. De Dominicis, J. Phys. C **15**, 7165 (1982).
[35] A. Crisanti and T. Rizzo, Phys. Rev. E **65**, 046137 (2002).
[36] M. Mézard, G. Parisi, and M. A. Virasoro, *Spin Glass Theory and Beyond* (World Scientific, Singapore, 1987), Chap. 4.
[37] F. Pázmándi, G. Zaránd, and G. T. Zimányi, Phys. Rev. Lett. **83**, 1034 (1999).
[38] P. Le Doussal, M. Müller, and K. J. Wiese, Europhys. Lett. **91**, 57004 (2010).
[39] A. Sharma, A. Andreanov, and M. Müller, Phys. Rev. E **90**, 042103 (2014).
[40] W. Ching and D. Huber, Phys. Lett. **59A**, 383 (1976).
[41] G. Schehr, Phys. Rev. B **71**, 184204 (2005).
[42] L. F. Cugliandolo and M. Müller, Quantum glasses—A review, *Spin Glass Theory and Far Beyond* (World Scientific, Singapore, 2023), Chap. 18.
[43] S. Sachdev, N. Read, and R. Oppermann, Phys. Rev. B **52**, 10286 (1995).
[44] N. Kavokine, H. Lu, N. Wentzell, and O. Parcollet, https://github.com/TRIQS/ctseg.
[45] N. Kavokine, M. Müller, A. Georges, and O. Parcollet (2024), 10.5281/zenodo.10475973.